APPLIED SCIENCES AND ENGINEERING

Enhanced interfacial electron transfer between thylakoids and RuO_2 nanosheets for photosynthetic energy harvesting

Hyeonaug Hong[1†], Jang Mee Lee[2†], JaeHyoung Yun[1], Yong Jae Kim[1], Seon Il Kim[1], HyeIn Shin[1], Hyun S. Ahn[3], Seong-Ju Hwang[4]*, WonHyoung Ryu[1]*

The harvesting of photosynthetic electrons (PEs) directly from photosynthetic complexes has been demonstrated over the past decade. However, their limited efficiency and stability have hampered further practical development. For example, despite its importance, the interfacial electron transfer between the photosynthetic apparatus and the electrode has received little attention. In this study, we modified electrodes with RuO_2 nanosheets to enhance the extraction of PEs from thylakoids, and the PE transfer was promoted by proton adsorption and surface polarity characteristics. The adsorbed protons maintained the potential of an electrode more positive, and the surface polarity enhanced thylakoid attachment to the electrode in addition to promoting ensemble docking between the redox species and the electrode. The RuO_2 bioanode exhibited a five times larger current density and a four times larger power density than the Au bioanode. Last, the electric calculators were successfully powered by photosynthetic energy using a RuO_2 bioanode.

INTRODUCTION

Photosynthesis is one of the most efficient energy conversion processes that exist in nature, where the quantum efficiency of the number of oxygen molecules produced from water splitting by photon absorption is known to be close to 100% (*1*, *2*). Photosynthesis occurs in the thylakoid membranes (TMs) within the chloroplasts of photosynthetic plants, algae, or bacteria. The thylakoids contain photosynthetic apparatus such as photosystem II (PSII), the plastoquinone (PQ) pool, cytochrome b_6f (Cyt b_6f), plastocyanin (PC), and PSI. Initially, in PSII, photosynthetic electrons (PEs) are generated by water splitting, and using the energy of the incident photons, they become high-energy PEs (photosynthetic Z scheme). The PEs are then transported through sequential redox reactions by electron carriers such as PQ, Cyt b_6f, and PC in the PE transport (PET) chain. Subsequently, the PEs are transferred to the acceptor site of PSI by PC and are excited by the incident photon energy. Last, ferredoxin (FD) oxidizes PSI and migrates to reduce nicotinamide adenine dinucleotide phosphate ($NADP^+$) to NADPH, which is ultimately used in the synthesis of carbohydrates.

To date, various attempts have been made to extract PEs from photosynthetic microorganisms, including algae (*3*–*6*) and cyanobacteria (*7*–*10*) or purified photosynthetic complexes, including PSI (*11*–*17*), PSII (*15*, *18*–*20*), and TMs (*21*–*34*). Although algae and cyanobacteria are highly stable and capable of generating PEs, the use of mediators and uncontrolled proliferation of cells is disadvantageous. Instead, when isolated photosystems are used, a much higher photosynthetic energy density can be obtained compared to the algae/bacteria approach. However, the instability of PSII and the need for electron donors for PSI result in limitations for these systems. In contrast, TMs are advantageous because of their simple isolation process, their stability over several days or longer, and the variety of sources available for PE extraction. Thus, when TMs are used, PEs can be extracted from a variety of electron carriers in PET chains, such as PSII, PQ, Cyt b_6f, PC, or PSI (*35*).

To extract PEs, the potential of the electrode surface should be maintained more positive than the redox potential of the electron donor sites of the photosystems or electron carriers. In this process, PEs can be transferred only when the redox species are completely attached or very close to the electrode, and so, if they are located far from the electrode, then the transfer of PEs is limited. This physical contact is influenced by the electrostatic or hydrophilic attractions between the electron carrier and the electrode, and these conditions play a particularly important role in interfacial electron transfer (*36*–*38*). Thus, to improve direct PE transfer, including electron transfer by endogenous electron carriers without considering electron transfer by artificial mediators, several studies have been carried out to reduce the physical distance by generating chemical bonds between the photosynthetic complexes and the electrodes (*7*, *8*, *11*, *21*, *24*, *33*, *39*). However, these strategies still have limitations in that the fabrication of chemical bonding is too complicated, and the chemically bonded length is too long for direct PE transfer (*40*). Studies have also been conducted to increase the amount of extracted PEs by injecting artificial mediators that can shuttle PEs from the redox species to the electrodes (*8*, *10*, *12*, *21*, *23*). However, although these methods show increased photosynthetic current densities, the artificial mediators used are associated with environmental toxicity and electrical potential loss.

For these reasons, the direct extraction of PEs from the PET chain without artificial mobile mediators has been pursued to achieve highly efficient and stable PE harvesting. A key issue in direct PE extraction is the lack of an understanding as to how PEs can be extracted from the photosynthetic apparatus to the electrode surface (anode). Previous studies have reported increased PE collection by

[1]Department of Mechanical Engineering, Yonsei University, Seoul 03722, Republic of Korea. [2]Global Innovative Center for Advanced Nanomaterials (GICAN), School of Engineering, Faculty of Engineering and Built Environment, The University of Newcastle, Callaghan, NSW 2308, Australia. [3]Department of Chemistry, College of Science, Yonsei University, Seoul 03722, Republic of Korea. [4]Department of Materials Science and Engineering, College of Engineering, Yonsei University, Seoul 03722, Republic of Korea.
*Corresponding author. Email: whryu@yonsei.ac.kr (W.R.); hwangsju@yonsei.ac.kr (S.-J.H.)
†These authors contributed equally to this work.

attaching PSII, PSI, and TMs to various electrodes with tethering chemical linkers (*7*, *21*). However, despite improved performances, the mechanisms of PET from the photosynthetic apparatus through the linkers to the electrodes have yet to be clearly explained.

In this study, we propose a two-dimensional (2D) ruthenium dioxide (RuO_2) nanosheet (NS)–modified electrode to increase the amount of PE extracted from thylakoids (Fig. 1). RuO_2 NSs are known to adsorb protons inside their lattice in an aqueous solution, which leads to the potential of the RuO_2 electrodes becoming more positive than that of an Au electrode (Fig. 1B) (*41*–*43*). In addition, because of the fact that RuO_2 NSs have locally varying positive and negative surface charges, TMs bearing negative surface charges due to the presence of carboxyl groups and/or the phosphate groups of proteins (and a small portion of sulfo- and phospholipids) can be firmly attached to the positively charged region of the NS surfaces by electrostatic attractions (Fig. 1C) (*44*, *45*). Such heterogeneous distribution of the surface charges also allows for the ensemble docking of photosynthetic proteins to the matching spot on the electrode surface, and the metal-like high-electrical conductivity of the RuO_2 NS facilitates highly efficient PET from the photosynthetic proteins to the electrode regardless of their surface charges (Fig. 1D) (*41*). Thus, we report the preparation of RuO_2 NS–modified electrodes (RuO_2 electrodes) by electrophoretic deposition and subsequent demonstration of their enhanced functionality as biophotoanodes. In addition, the PE extraction capability of the RuO_2 electrodes bearing thylakoids (RuO_2 bioanodes) is compared with that of Au bioanodes. Last, photosynthetic electrochemical cells are constructed using the RuO_2 bioanodes, and the operation of a small calculator by photosynthetic energy through the connection of multiple cells is investigated.

RESULTS

Fabrication of the RuO_2 electrodes

Exfoliated RuO_2 NSs were prepared by the chemical exfoliation of layered α-$NaRuO_2$ structures, as reported previously (*46*). Transmission electron microscopy images of the obtained RuO_2 NSs showed a 2D sheet-like morphology with faint contrast, confirming successful exfoliation into monolayered 2D RuO_2 NSs with lateral sizes of several hundred nanometers and a subnanometer level thickness. The exfoliated RuO_2 NSs appeared negative in the zeta potential analysis, indicating their anionic surface. To modify the electrodes with RuO_2 NSs, two deposition methods were investigated, namely, drop-casting and electrophoresis (see section S2). In both cases, similar photosynthetic currents were observed. However, the RuO_2 NS film fabricated by drop-casting was nonuniform and easily detached upon immersion in an aqueous solution (fig. S2). On the other hand, electrophoresis resulted in the more uniform modification of the electrode with NSs, thereby leading to faster and more stable electron transfer. On the basis of these results, we selected electrophoretically modified electrodes for use in this study.

Deposition of the thylakoid films

The processes used for thylakoid purification and measurement of the chlorophyll concentration are described in Materials and Methods. An aliquot (30 μl) of the thylakoid solution with a chlorophyll concentration of 2 mg ml^{-1} was drop-casted onto an Au electrode and a RuO_2 electrode for photosynthetic current measurements. After 3 hours of drying, the thylakoids formed 5- to 10-μm-thick films on the electrodes (fig. S3, A and B). To attach thylakoids to the RuO_2 NS, the drop-casted thylakoid solution was dried to physically attach the thylakoids to the electrode. Since thylakoid drying for

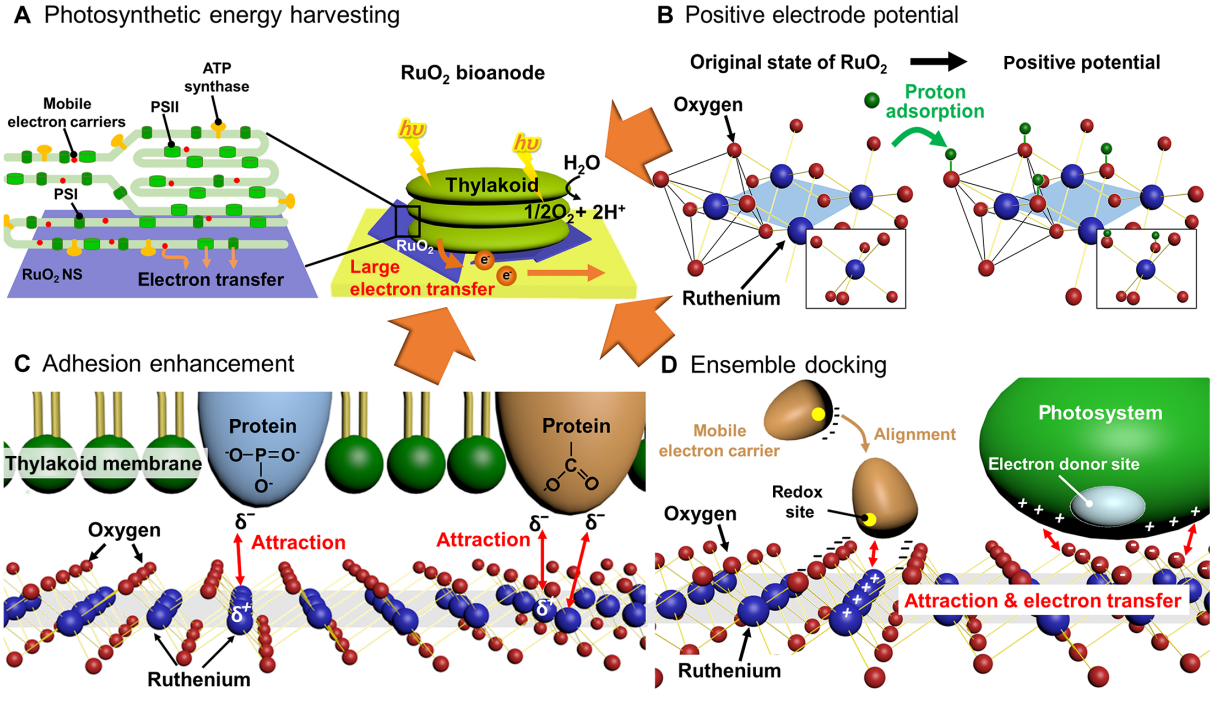

Fig. 1. Enhanced interfacial electron transfer through RuO_2 NSs. (**A**) Schematic of PE harvesting with RuO_2 bioanode. ATP, adenosine 5′-triphosphate. (**B**) Proton adsorption characteristic of RuO_2 NS result in positive electrode potential. (**C**) Adhesion enhancement by electrostatic interactions between RuO_2 NS and TMs. (**D**) Ensemble docking induced by RuO_2 NS to electron carrier and PS.

long periods may damage the thylakoid performance, the drying time was set to a maximum of 3 hours. In the presence of 2,6-dichlorophenolindophenol (DCPIP), the absorbance of the dried thylakoid at 600 nm decreased because of the reduction of DCPIP, and so, it was confirmed that the photosynthetic activity of the drop-casted thylakoid had been maintained (fig. S4).

Thylakoid adhesion to the electrodes

To confirm the adhesion between the thylakoids and the electrode surfaces, dried thylakoids were eliminated by rigorous washing with deionized water and N_2 blowing. In the case of the bare Au electrode, the drop-casted thylakoids were found to be successfully washed off (fig. S3, C and D). In contrast, the thylakoids remained firmly attached to the RuO_2 electrode surface after washing (fig. S3, E and F). Most of the thylakoids were located close to the RuO_2 NSs, which can be observed as a wrinkled structure in fig. S3F. This was due to the fact that the partially positively charged surfaces of the RuO_2 NSs enhanced adhesion of the TM to the electrode, thereby preventing their detachment from the electrode despite thorough washing.

Electrode potential of the RuO_2 electrode

One of the important roles of RuO_2 NSs in PE harvesting is proton adsorption, which results in a more positive electrode potential. As shown in Fig. 2, RuO_2 electrodes have a more positive potential than Au electrodes, which is beneficial in the context of extracting PEs from thylakoids during photosynthesis. More specifically, the electron carriers in the PET chain are more attracted when the electrical field is strong. Considering the electronegativities of the Ru and O atoms, it would be preferable for protons to be adsorbed close to the O atoms rather than the Ru atoms in the RuO_2 lattice. Proton adsorption in the vicinity of the O atoms in the RuO_2 NSs can be clearly evidenced by Ru K-edge extended x-ray absorption fine structure (EXAFS) analysis for the RuO_2 NSs both in the presence and absence of an electrolyte. As shown in fig. S5, soaking in the electrolyte leads to a slight decrease in the oscillation wavelength in the EXAFS oscillation, reflecting an increase in the Ru-O bond distance. This is further confirmed by the distinct shift in the Fourier transform (FT) peak at ~1.7 Å, corresponding to a longer Ru-O bonding shell upon soaking in the electrolyte. The elongation of the Ru-O bond distance in the electrolyte can be interpreted as strong evidence for proton adsorption on the O atom, since the newly created O-H^+ interaction weakens the neighboring Ru-O bond via the bond competition effect. To quantitatively estimate the local structural evolution of the RuO_2 NSs caused by the electrolyte, fitting analysis was carried out for the obtained EXAFS spectra, as outlined in table S1. Because of the uncertainty of the bond distance (R) estimated from EXAFS fitting analysis (±0.01 Å), the RuO_2 NSs soaked in an electrolyte exhibit distinctly longer Ru-O bond distances than in the absence of an electrolyte, thereby confirming elongation of the Ru-O bond upon proton adsorption. Upon integration of the TM with the RuO_2 NSs, this phenomenon of proton absorption leads to the remarkable facilitation of electron extraction from the TM, thereby preventing charge accumulation in the RuO_2 NS.

On the other hand, the potentials of the thylakoid-deposited Au and RuO_2 bioanodes are more negative than before thylakoid deposition (Fig. 2A), and this is due to the potential formed by the photosystems or electron carriers of the TMs contacted on the electrode. Because of the fact that the most positive redox potential of the electron carriers on the PET chain is <200 mV (the redox potential of PC is

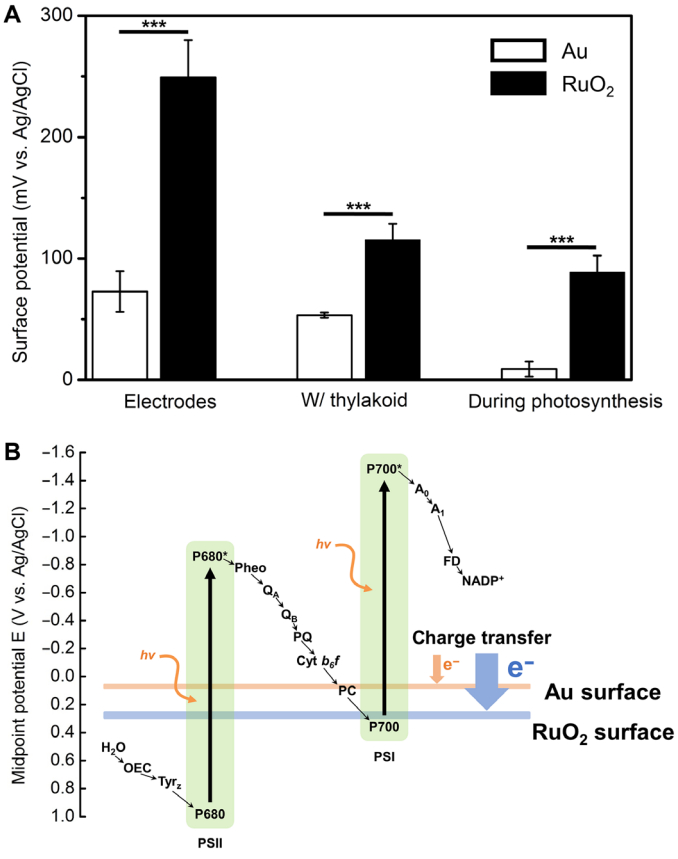

Fig. 2. Electrode potential of electrodes. (**A**) Electrode potential of Au and RuO_2 electrodes without and with thylakoid and during PEs harvesting. ***Student's t test, $P < 0.001$ and $n = 5$ for statistical analysis. (**B**) Midpoint potential of electron carriers on PET chain of thylakoid. Oxygen evolution complex (OEC), tyrosine (Tyr_z), pheophytin (pheo), primary and secondary acceptor quinone (Q_A and Q_B), chlorophyll (A_0), and pylloquinone (A_1).

160 mV versus Ag/AgCl), enhanced PE extraction is possible using the RuO_2 electrodes (Fig. 2B).

Since the proton adsorption behavior of RuO_2 is related to its pseudocapacitance, we subsequently investigated the supercapacitive characteristics of the RuO_2 electrodes. In previous studies, Pankratova *et al.* and Santoro *et al.* (*24*, *47*) reported that an enhanced capacitance can improve the current density of a photobioanode by reducing the impedance of the electrode. Figure S6 shows the cyclic voltammograms of the RuO_2 and Au electrodes in the presence of 100 mM potassium nitrate in phosphate-buffered saline (PBS). The capacitances calculated from the cyclic voltammograms were 11.5 μF cm^{-2} for the Au electrode and 101.6 μF cm^{-2} for the RuO_2 electrode. This supercapacitive nature of the RuO_2 electrode is likely to explain the sharper increase in PE currents upon illumination compared to the onset behavior of the PE currents collected by the Au electrode (Fig. 3A).

Extraction of PEs

To investigate the effect of the NSs on the photocurrents, the photoelectric currents were measured without thylakoid loading on the Au and RuO_2 electrodes. Figure S7 shows that upon examination of the magnitudes of the photosynthetic currents, the photoelectric currents were sufficiently small to be considered negligible. With

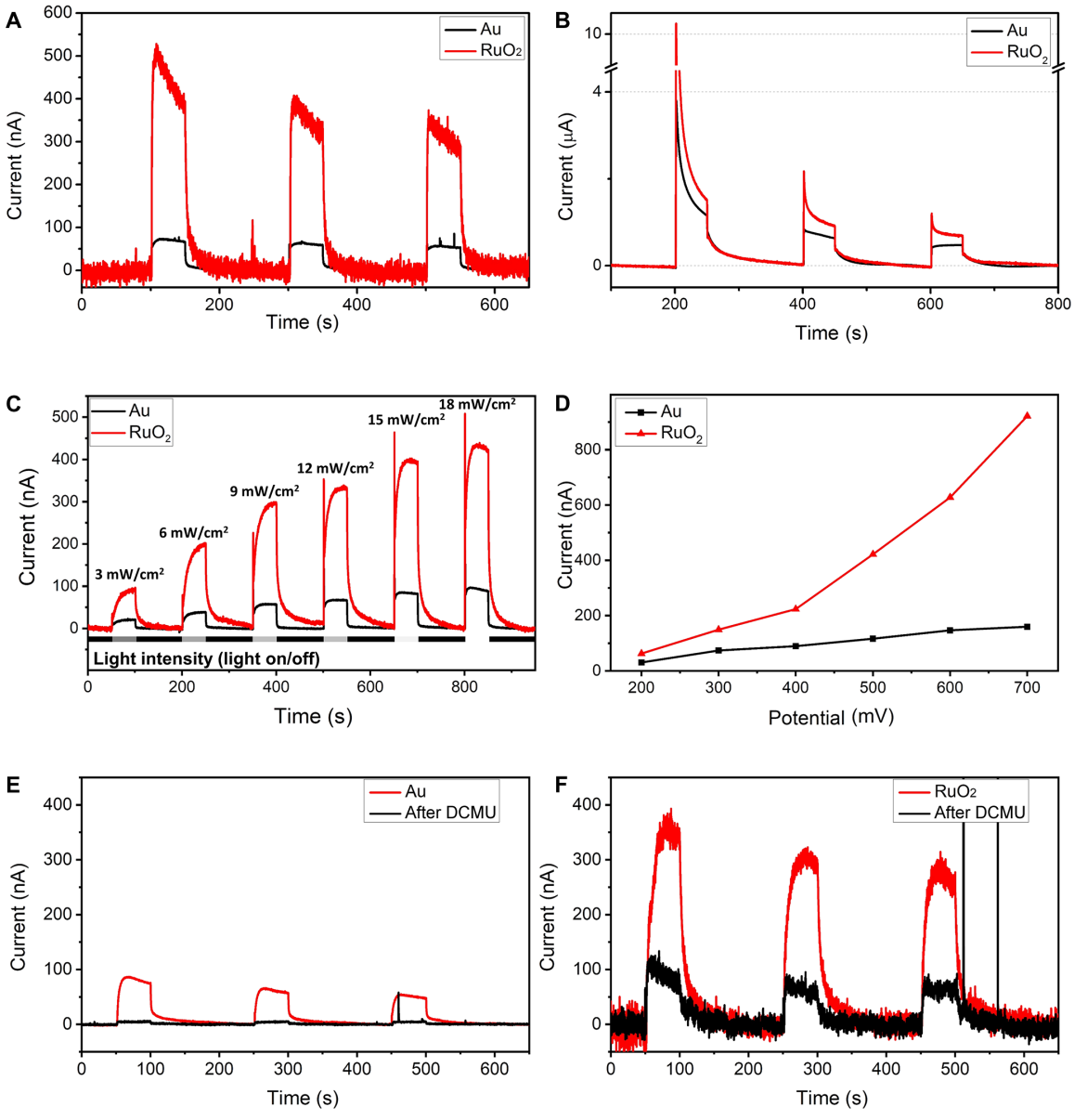

Fig. 3. Photosynthetic currents measured from Au and RuO_2 bioanodes. (**A**) Photosynthetic currents with 10 mW cm^{-1} of light intensity and 400 mV of bias potential. (**B**) Mediated PEs harvesting through potassium ferricyanide. (**C**) PE currents depending on light intensity with 400 mV bias potential. (**D**) Dependency of PE currents on the bias potential with 10 mW cm^{-1} of light intensity. Photosynthetic current before and after 1 mM 3-(3,4-dichlorophenyl)-1,1-dimethylurea (DCMU) addition to (**E**) Au bioanode and (**F**) RuO_2 bioanode.

thylakoid deposition on each type of electrode, photosynthetic currents of 70 and 500 nA were measured for the Au and RuO_2 bioanodes, respectively (Fig. 3A). This result can be attributed to the positive electrode potential of the RuO_2 bioanode compared to that of the Au bioanode, as well as the surface polarity of the RuO_2 electrodes. As previously mentioned, since a more positive electrode can extract a larger amount of PEs from thylakoids, the RuO_2 bioanode exhibited larger PE currents than the Au bioanode. Surface polarity is another important property of RuO_2 NSs, which can influence the adhesion and ensemble docking between the electron carriers and the electrodes. Enhanced adhesion can reduce the distance between the thylakoids and the electrodes, which, in turn, facilitates the transportation of PEs to the electrodes. The partially positively and negatively charged surfaces of RuO_2 NSs can induce ensemble docking, which improves the efficiency of PE transfer by attracting greater numbers of electron carriers from the thylakoids regardless of whether their surfaces are negatively or positively charged. This will be discussed further in Discussion.

To better understand the mechanism behind the enhancement in PE extraction, a mediator was added to the system, and the photosynthetic currents were measured for both the Au and the RuO_2 bioanodes. If the increase in PE currents is due only to the enhanced contact between photosynthetic proteins and the RuO_2 electrode, then the magnitude of the PE currents from both the Au and RuO_2

electrodes should be similar when a sufficient mediator is present. More specifically, sufficient artificial mediators can shuttle almost all PEs to the electrode surface from the thylakoids, even those that exhibit a weak adhesion or exist far from the electrode surface. To verify this hypothesis, 30 mM potassium ferricyanide as a mediator and 300 mM potassium nitrate as a supporting medium were added to the solution. The photosynthetic currents (first peak) in the presence of the artificial mediator increased by more than 10 times for both the RuO_2 and the Au bioanodes. This was attributed to the initially high concentration of the mediator close to the electrode, which decreases as the redox reaction progresses because of diffusion limitations (*21*). Note that the magnitude of the PE current from the RuO_2 bioanode was higher than that from the Au bioanode (Fig. 3B). This additional enhancement can be explained by considering the supercapacitor-like behavior of the RuO_2 NSs and the more positive electrode potential compared to that of the Au bioanode due to the proton adsorption characteristics of the RuO_2 NSs. As shown in Fig. 2, in addition to the surface polarity effect, the potential of the electrode also plays an important role in extracting greater quantities of PEs.

Since intense light can produce greater quantities of PEs from thylakoids, the photosynthetic currents resulting from different light intensities were investigated. Thus, Fig. 3C shows the photosynthetic currents achieved using 3, 6, 9, 12, 15, and 18 mW cm^{-2} of input light power. With 3 mW cm^{-2} of light power, photosynthetic currents of 20.8 and 92 nA were measured for the Au and RuO_2 bioanodes, respectively, while currents of 93 nA from the Au bioanode and 426 nA from the RuO_2 bioanode were recorded with a light intensity of 18 mW cm^{-2}. Although the photosynthetic currents increased upon increasing the intensity of the light power, the ratio of the currents measured for the two bioanodes remained relatively constant. The potential of an electrode is also an important parameter for extracting PEs from thylakoids. When the bias voltage is large, PEs are more strongly attracted to the electrode, resulting in larger PE currents (Fig. 3D). To confirm whether the current generated by light is a photosynthetic current, we added a Q_B site inhibitor, namely, 3-(3,4-dichlorophenyl)-1,1-dimethylurea (DCMU), to the Au and RuO_2 bioanodes (Fig. 3, E and F). More specifically, when 1 mM DCMU was added to the PBS solution, almost no photosynthetic current was measured for the Au bioanode, while a noticeable residual current was observed for the RuO_2 bioanode. To investigate the possibility that Q_B was not inhibited because of the slow diffusion of DCMU, samples of DCMU-treated thylakoids before drop-casting were also measured (fig. S8). However, the RuO_2 bioanode still exhibited a residual current, and the magnitude of the current was not considerably different from the previous result. Such a residual current after DCMU treatment was also observed in the PSII-decorated indium tin oxide electrode, which therefore indicates that electron transfer from Q_A to the electrode is possible (*48*, *49*). It is likely that the remaining photocurrents after DCMU inhibition originated from the Q_A sites of PSII, the noninhibited PSII, Cyt b_6f, or PSI. Thus, to further understand the origin of the photocurrents, $ZnCl_2$ was also applied as a Cyt b_6f inhibitor (fig. S8). It was found that the magnitude of the photocurrents was larger in the case of $ZnCl_2$ inhibition than when DCMU was used. This indicates that the different photocurrents obtained upon DCMU and $ZnCl_2$ inhibition originate from PSII or from the PQ pool. These results are also consistent with those reported by Rasmussen and Minteer (*50*).

In situ x-ray absorption spectroscopy analysis during the photosynthetic process

To understand the mechanism responsible for the substantial improvement in the photosynthetic properties of TMs upon the use of RuO_2 NSs as an electrode-modifying metal oxide, in situ EXAFS analysis was performed for RuO_2-thylakoid and bare RuO_2 films under light illumination, as shown in fig. S9. An anodic potential of 0.4 V was applied for both films under the same conditions as those used in the previous photosynthetic current tests. Figure 4 illustrates the Fourier-filtered k^3-weighted Ru K-edge EXAFS oscillations and their FT data for the RuO_2-thylakoid and RuO_2 films before and after light illumination, respectively. As shown, light irradiation of the RuO_2 film induces a slight increase in the oscillation wavelength, suggesting a shortening of the Ru-O bond distance, whereas a negligible change was observed for the RuO_2-thylakoid film upon light irradiation. As shown in Fig. 4 (C and D), both films display typical FT features of the α-$NaRuO_2$ crystal phase consisting of Ru-O and edge-shared Ru-Ru bonds at ~1.7 and ~2.8 Å, respectively. While the RuO_2-thylakoid film exhibit nearly identical FT peaks even after light illumination, a minute but distinct difference is observed for the RuO_2 film, which shows distinct shortening of the Ru-O bond distance under light illumination. The observed shortening of the Ru-O bond distance for the bare RuO_2 film suggests the occurrence of a slight increase in the Ru oxidation state, which can be ascribed to the removal of electrons from the RuO_2 NSs under light irradiation due to the photoelectric effect. On the other hand, the negligible change in the Ru-O bond distance for the RuO_2-thylakoid film under light illumination can be interpreted as an offset of the photoinduced electron depletion by electron injection from the intimately coupled thylakoid species (Fig. 1). Notably, in contrast to the first FT peak, light illumination of the bare RuO_2 film induces a notable intensity enhancement for the second FT peak related to the Ru-Ru bond, which reflects an improvement in the structural order. This is attributable to an increase in the Ru oxidation state upon light illumination, which, in turn, results in an enhanced stability for the RuO_2 lattice, and the depression of structural disorder. This phenomenon was not discernible for the RuO_2-thylakoid film, which exhibited no change in the Ru oxidation state upon illumination. The unique characteristics of 2D NSs, such as an unusually high anisotropic structure, a molecularly thin nature, and a large surface area, enable the facile access and concomitant adsorption of protons to the RuO_2 lattice. To quantitatively estimate the local structural evolution before and after light illumination, a fitting analysis was carried out for the obtained EXAFS spectra, as shown in table S2 and fig. S10. The RuO_2 film exhibits a distinct shortening of the Ru-O bond under light illumination, while light irradiation has a negligible effect on the Ru-O bond distance of the RuO_2-thylakoid film. In addition, we could accurately estimate the evolution of the coordination number (CN) upon thylakoid immobilization using the amplitude reduction factor (S_0^2) obtained from the reference RuO_2 NSs with a CN of 6 because the calculated CN from the EXAFS fitting analysis corresponds to the product of the real CN and S_0^2 values. As outlined in table S1, the RuO_2-thylakoid has a notably larger CN value (6.8) than that of the bare RuO_2 film, which could be interpreted as clear evidence for the formation of additional interfacial coordination bonding between the Ru ions of the RuO_2 NSs and the proteins of the thylakoid. Such formation of interfacial coordination bonding between the RuO_2 NSs and the thylakoid is effective in promoting internal

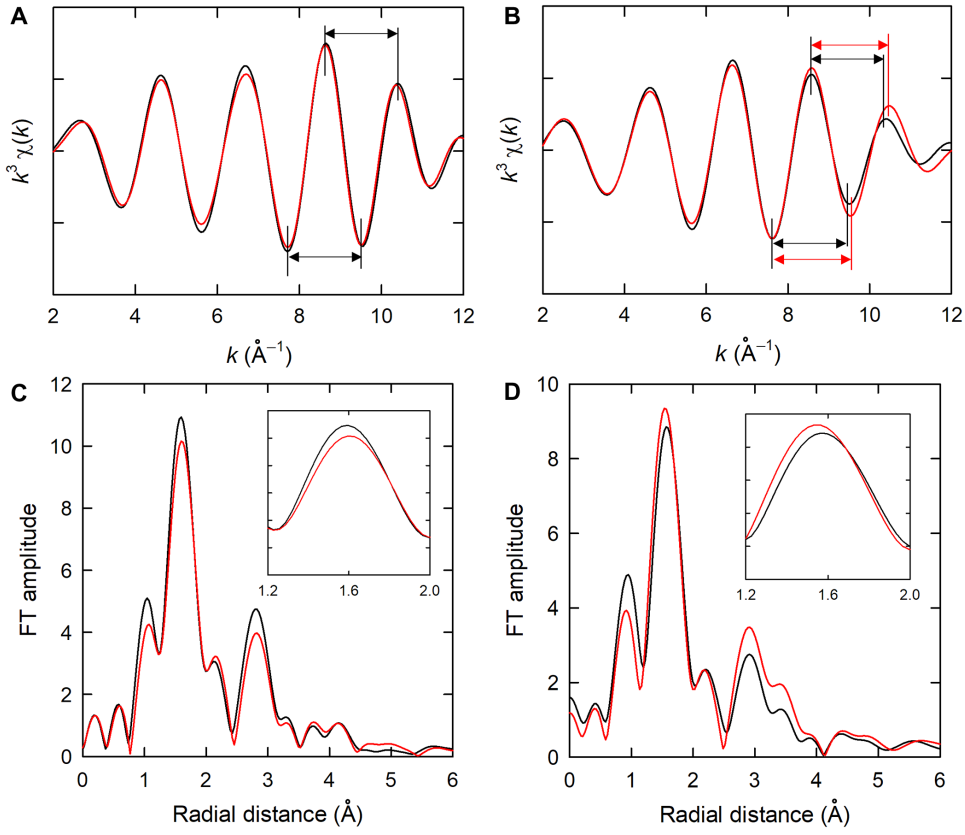

Fig. 4. Fourier-filtered k^3-weighted Ru K-edge EXAFS oscillations and their FT data. (**A** and **B**) In situ Fourier-filtered Ru K-edge EXAFS data and (**C** and **D**) their FT of the (A and C) RuO_2-thylakoid and (B and D) RuO_2 films before (black) and after (red) the light illumination.

charge transfer in the RuO_2-thylakoid film via the inner sphere mechanism.

To precisely characterize the nature of the electrode interface, we also carried out variable-angle spectroscopic ellipsometry. The refractive index (n) and extinction coefficients (k) for the RuO_2 and thylakoid layers were measured as a function of the wavelength (fig. S11). Between the RuO_2 and thylakoid layers, there is an additional interface layer whose refractive index and extinction coefficients are quite different from those of RuO_2 and the thylakoid layers. Note that this interface layer displays a relatively higher extinction coefficient, which could be beneficial for boosting light absorption and electron transfer (*51*).

Photosynthetic electrochemical full cell

To attempt the harvesting of photosynthetic energy, an electrochemical full cell was constructed with a photosynthetic bioanode and an air-breathing cathode (Fig. 5A). PEs produced and harvested at the bioanode are consumed to form water at the cathode by the oxygen reduction reaction (ORR). The cell performance was tested by linear sweep voltammetry from the open circuit voltage (OCV) to 0 V using a potentiostat (Fig. 5B). The short circuit current and maximum power from RuO_2 bioanode were determined to be 8.84 μA cm^{-2} and 0.74 μW cm^{-2}, respectively, whereas values of 4.70 μA cm^{-2} and 0.39 μW cm^{-2} were obtained for the Au bioanode. In addition, the OCVs of the RuO_2 and Au bioanodes are measured as 424 ± 17.2 and 575.1 ± 6.7 mV, respectively. This is due to the fact that the potential of the RuO_2 bioanode is closer to the ORR potential of the air-breathing cathode than that of the Au bioanode. Although the OCV of the RuO_2 bioanode is small, its maximum power is four times higher than that of the Au bioanode owing to the large current. To confirm the effect of light intensity on the cell power, the intensity was controlled from the level of laboratory light (10 mW cm^{-2}) to strong sunlight (100 mW cm^{-2}). As shown in Fig. 5D, the cell power increased noticeably upon increasing the light intensity.

To confirm the potential of photosynthetic energy harvesting, the photosynthetic electrochemical cells were connected to a small calculator that was originally operated by a 3-cm^2 solar cell panel. Eight cells, each with an area of 1.7 cm^2, were connected in parallel as a pair (one set), and four sets were connected in series to form a circuit (Fig. 6A). The constructed circuit exhibited an OCV > 1.4 V, which is sufficient to operate the calculator. The onset voltage of the calculator was measured as 1.28 V, and when the voltage was greater than the onset voltage, it turned on automatically. If the current fell below 1 μA during operation, then the displayed digital numbers became very dimmed, and when the current or voltage values dropped below 400 nA or 0.77 V, respectively, the calculator shut down and the circuit was opened, thereby resulting in an increase in the OCV through recharging. Even in the absence of photosynthesis, the OCV increased because of the movement of ions in the solution, although a time of approximately 11 min was required to reach 1.2 V (Fig. 6D). At this time, when the calculator was turned on, the current remained close to zero with the exception of the peak current attributed to button pressing, and so, the calculator was shut down within a few seconds (Fig. 6F, fig. S12, and movie S1). However,

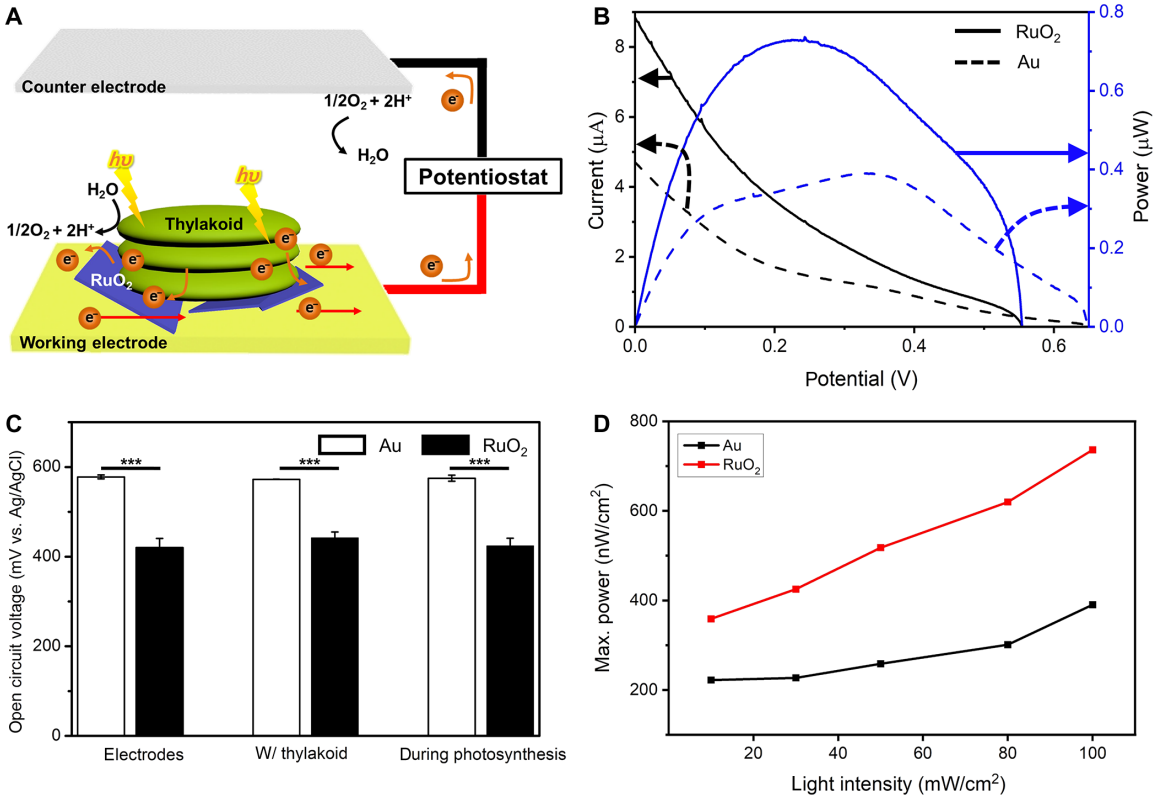

Fig. 5. Photosynthetic electrochemical cell for energy harvesting. (**A**) Schematic of photosynthetic energy harvesting. (**B**) Polarization curve of cells during photosynthesis. (**C**) OCV of cells. ***Student's *t* test, $P < 0.001$ and $n = 5$ for statistical analysis. (**D**) Dependency of maximum power on the light intensity.

in the presence of photosynthesis, the OCV charged more rapidly than in the absence of photosynthesis (i.e., 5 min and 30 s to reach 1.2 V, compared with ~10 min to reach 1.26 V), and the leakage current was ~100 nA at 1.26 V in the off state of the calculator (Fig. 6, D to F). Such fast charging under illumination is mostly due to the PEs from the thylakoid, and the fact that some RuO_2 NSs may have the possibility of charging through the photoelectric effect. When the calculator was turned on, the voltage dropped rapidly owing to the current flow (fig. S12 and movie S2). The current then slowly decreased from a few microamperes to 400 to 500 nA for a few minutes, and the current flow stopped when the calculator was completely powered off. To increase the OCV before switching on the calculator, the cells were disconnected from the calculator so that the leakage current was suppressed (Fig. 6H). In this case, the OCV gradually increased to >1.4 V, and after the cells were connected, it was possible to operate the calculator for more than 30 s because of the presence of this stored energy (movie S3).

DISCUSSION

Over the past decade, although many studies have been reported in the area of photosynthetic energy harvesting, the amount of extracted PEs is still limited, and the durability of the system is too short. To improve the extraction of PEs, electrochemical mediators have been used to enhance electron transfer between photosynthetic complexes and electrodes; however, the use of mediators has undesirable side effects, such as energy loss during redox reactions, environmental toxicity, and instability due to exposure to light and temperature (*52*, *53*). For direct PE extraction, photosynthetic complexes have been immobilized on an electrode by chemical tethering or drop-casting, and improved stabilities were demonstrated (*18*, *53*). In addition, Sekar *et al.* and Calkins *et al.* (*7*, *21*) reported a further improvement in PE extraction by the use of chemically tethered thylakoids or cyanobacteria in the presence of mediators. Although these studies improved PE harvesting by electrochemically shortening the connection between the photosynthetic complexes and the electrodes, the mechanisms related to PE transportation between electron carriers were not discussed in detail in any previous words.

Our present study began with the hypothesis that the modification of electrodes based on the fundamental mechanisms of electron transfer between electron carriers and an electrode can facilitate PE extraction from thylakoids. Electron carriers in thylakoids have a hydrophilic or hydrophobic surface with a positive or negative charge, and these surface characteristics induce ensemble docking to transport PEs between themselves (*36*). More specifically, electron carriers are aligned and adhere to their specific redox sites via electrostatic attractions induced by their surface charges. Subsequently, PEs can be transferred from the electron carriers with higher redox potentials to those with lower redox potentials upon physical contact. In the microscopic view of electron transfer, a distance shorter than 1.7 nm allows electron transfer by the tunneling effect (*54*). When the sizes of electron carriers are considered, all electron transfers between electron carriers are regarded as a result of the tunneling effect. When the PEs are extracted through electrodes, if the distance between the electrodes and the redox sites of the electron carriers is longer than 1.7 nm, then electrons must be

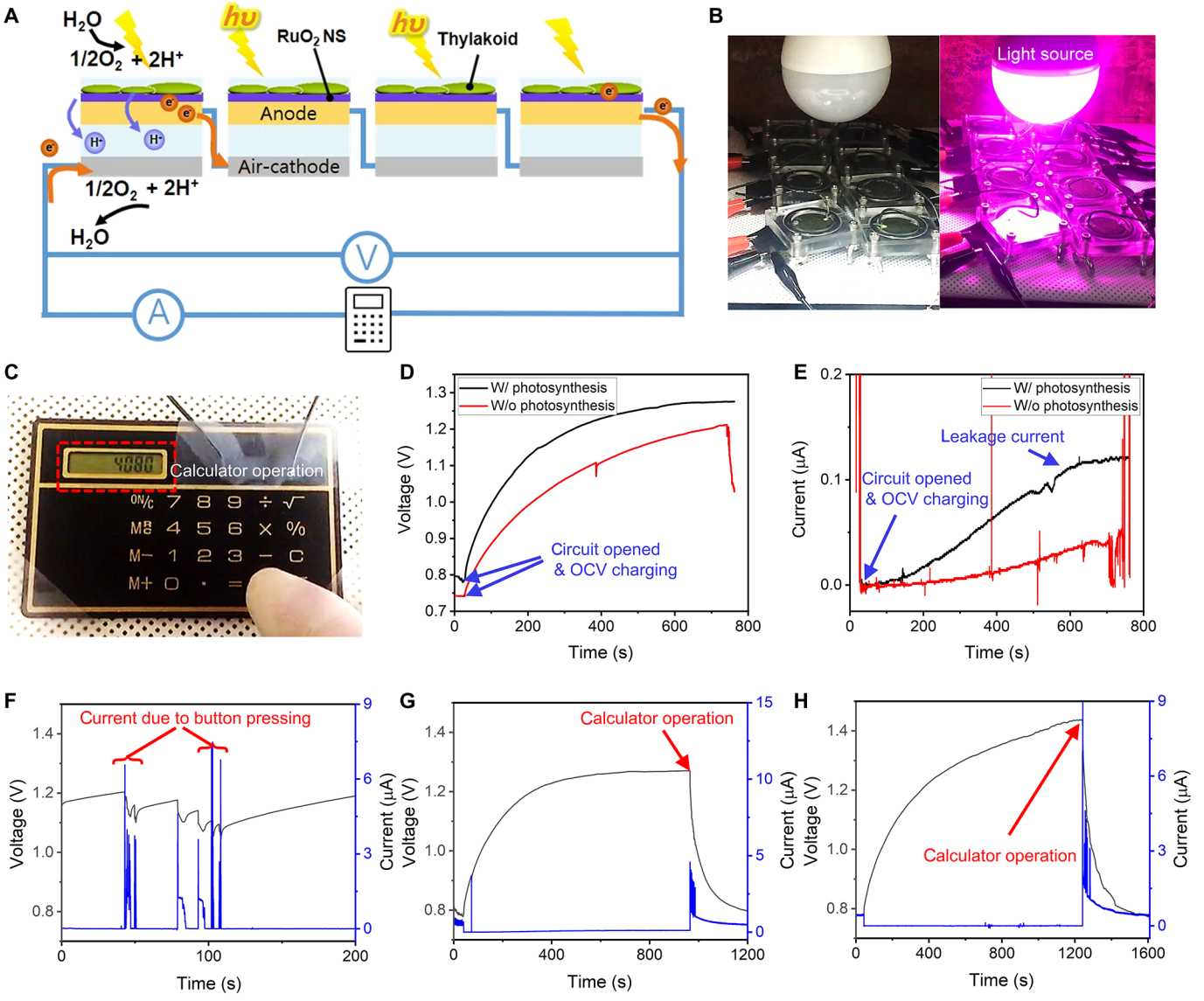

Fig. 6. Performance of the multiple connected photosynthetic electrochemical cells to operate a small calculator. (**A**) Conceptual figure of multiple connected photosynthetic electrochemical cells. (**B**) Images of cells under light off (left) and on (right). (**C**) The captured image of the calculator used here. (**D**) OCVs with and without illumination when the calculator is off. (**E**) Currents under the same conditions as (D). (**F** to **H**) Voltage (left, black line) and current (right, blue line) graphs when the calculator is off and on (F) without illumination, (G) with illumination, and (H) after leakage current suppressing by disconnecting the calculator. Photo credit: Hyeonaug Hong, Yonsei University.

transferred through hopping (*40*). Therefore, when chemical tethering is attempted to immobilize photosynthetic complexes on the electrodes, the tethering molecules should be carefully selected.

In addition, the binding between photosynthetic complexes and electrodes is mainly through amide bonds, which can lead to two specific issues. First, when the tethering molecules bind to proteins other than the endogenous electron carriers, PEs must overcome the electrical barrier formed by the tethering molecules (which usually form a self-assembled monolayer on the electrode) to be transferred from the electron carriers to the electrodes. Thus, the tethering molecules hinder the transport of PEs. Second, if the electron carriers bind with the tethering molecules, the redox-active sites on the electrode surface are inactivated because of binding, resulting in a reduction of the electrochemically activated area (*55*). For continuous electron transfer, PE donors migrate to the electrode surface and need to diffuse out after electron transfer, such that another new set of PE donors can access the electrode surface. However, if oxidized molecules are bound on the electrode surface after PE transfer, then electron transfer cannot be cycled continuously at the same redox reaction rate.

Various materials such as bioelectrodes have also been studied to efficiently extract PEs. In the case of metals, which are widely studied as electrode materials, physical contact between the thylakoids and the electrodes is weak and unstable because the electron pool on a metal surface induces electrostatic repulsion with the negatively charged TMs. For carbon electrodes, electron transportation

is hindered by hydrophobic carbon surfaces owing to poor adhesion to hydrophilic TMs. Although some transparent metal oxides have been examined, most metal oxides have not been considered for application as bioanodes owing to their low conductivities. In our experiments, the photosynthetic currents from the RuO_2 bioanode were found to be twice as large as those from the bioanode modified with other metal oxide NSs, such as MoS_2, CoO_2, and MnO_2 (fig. S13). In this work, PE extraction was investigated using a RuO_2 electrode because it is known to be the most conductive metal oxide. 2D RuO_2 NSs can be easily deposited as a thin uniform film on any electrode through electrophoresis. Because of the fact that the multiple-stacked layers of NSs can reduce electron conductivity across the layers, the controlled formation of uniform and thin layers of RuO_2 NSs on an electrode by electrophoresis is beneficial.

As described above, the magnitude of the PE currents from the electrode deposited with a small amount of RuO_2 NSs was more than five times higher than the PE currents from the Au bioanode. This supports the hypothesis that both proton adsorption and the surface polarity of the RuO_2 NSs can improve PE extraction via a positive electrode potential, thylakoid attachment, and ensemble docking inducement. In terms of proton adsorption, although the electrode potential was maintained at 400 mV by a potentiostat during the experiments, the actual surface potential of the RuO_2 electrode could become more positive owing to the proton adsorption inside the RuO_2 NS lattice (Fig. 1B) (*41*, *42*). The surface polarity of the RuO_2 NSs can attract the electron donor sites of photosystems or endogenous electron carriers through electrostatic attractions. In the case of PSII, electron donor sites with a positive charge are located facing the stroma. For this reason, PSII can be attached to the negatively charged sites (i.e., the oxygen region) of the RuO_2 NSs through electrostatic attractions, and electrons can be extracted from PSII through the movement of Q_A and Q_B over a distance of ~1 nm (*48*, *49*, *56*, *57*). In particular, regarding the DCMU results presented in Fig. 3 (E and F), it is likely that RuO_2 bioanodes directly accept electrons from Q_A without the influence of DCMU application. Considering the same phenomenon observed in another metal oxide (i.e., indium tin oxide), it can be assumed that Q_A can transfer electrons to the electrode on the basis of the strong polarity of the metal oxide, which is positively charged. Similar to the case of PSII, PSI also has positively charged electron donor sites, and it is well known that electrons can be transferred from an electron donor site to an electrode (*13*, *14*, *17*, *54*, *58*–*61*). PC and FD, which are the endogenous electron carriers of the thylakoid with negatively charged redox sites, are preferably attracted to the positive regions of the NSs (i.e., the Ru site) (*62*–*68*). The sizes of the redox sites of these metalloproteins are ~3 nm, which is similar to or slightly smaller than the moving distance of oxygen atoms on the RuO_2 NS surface. During electrostatic attraction between the electrode and the electron carriers, the negatively charged redox site is aligned to the Ru atom located relatively inside the NS, avoiding the protruding oxygen atoms (i.e., ensemble docking). When the species become sufficiently close, the PEs are transferred through tunneling.

Despite a short operating time of several tens of seconds, this study shows the potential of photosynthetic energy harvesting through the operation of a low-powered calculator. Moreover, if a 3D electrode is used instead of the 2D planar electrode used in this study, it will be possible to obtain a higher current density because more PEs can be obtained from many thylakoids. The improved energy density is thought to be able to drive small devices, and it is expected to increase the range of applications when photosynthetic energy is used in combination with capacitors or batteries.

In this study, we developed RuO_2 electrodes for the direct extraction of PEs from thylakoids. It was found that the electrophoretic deposition of RuO_2 formed thinner and more stable films on the electrodes than when the drop-cast method was used. The resulting RuO_2 film enabled the electrode to exhibit a more positive potential and a higher surface polarity, which resulted in a larger amount of PEs being extracted from thylakoids compared to that in the case of the unmodified electrode. Last, a fuel cell was fabricated for photosynthetic energy harvesting, and it was demonstrated that multiple cells are able to operate a small calculator.

MATERIALS AND METHODS

Materials

All chemicals used in this work were purchased from Sigma-Aldrich Korea. To be specific, PBS (product no. P4417) was dissolved in distilled water (1 tablet per 200 ml, containing 10 mM phosphate buffer, 2.7 mM KCl, and 137 mM NaCl with pH 7.4), and this was used for the main solution of thylakoid purification and electrochemical measurements. PBS solution with sucrose (product no. S9378) was used for spinach blending and centrifugation. Magnesium chloride ($MgCl_2$; product no. M8266) was added in PBS solution to puncture chloroplast membrane by osmotic shocking. Sonicator (product no. Q125, tip product no. 4422, Qsonica, USA), ten broeck tissue grinder (product no. T24-132-575, Chemglass, USA), and centrifuge (Allegra X-15R and Optima XPN-100, Beckman Coulter, USA) were used for thylakoid purification. Potassium ferricyanide [$K_3Fe(CN)_6$; product no. 702587] and potassium nitrate (KNO_3; product no. P8394) were used to perform the cyclic voltammetry and fuel cell experiments. One-millimeter thickness of Boro-33 glass wafer as substrates of electrode was purchased from TPS (Republic of Korea). Silver paste (Elcoat, product no. P-100) was purchased for wiring between the electrodes and electric wire. Air-breathing cathode (product code SLGDE, FuelCellsEtc, USA) consisted of platinum (0.5 mg cm^{-2}) on Vulcan (60% on carbon) cloth with Nafion coating for ORR. The solar-powered calculator (Iaan Science, product no. P0000UHF) and the 15-W light-emitting diode bulb (ANP Electronics Co. Ltd., product no. GB130) were used to confirm the operating calculator.

RuO_2 NS fabrication

Exfoliated RuO_2 NSs were prepared as described in a previous study (*46*). The layered α-$NaRuO_2$ as pristine material was synthesized by a conventional solid-state reaction at 900°C for 12 hours. Then, stirring with 1 M $Na_2S_2O_8$ solution for 3 days led not only to elimination of interlayer Na ions but also to partial oxidation of Ru ions. Successive 3 days of reaction with 1 M HCl solution caused the interlayer distance of layered RuO_2 structure to increase slightly by replacing the interlayer Na ions with larger hydronium (H_3O^+) ions. Last, the colloidal suspension of successfully exfoliated RuO_2 NSs was obtained by reacting with a bulk tetrabutylammonium hydroxide solution for 10 days via an acid-base reaction.

Thylakoid purification

Thylakoids were purified from spinach by following the process. Fresh spinach was purchased from a local market. Only spinach

leaves were cut and selected from spinach, and then, leaves were washed by distilled water. Leaves (200 g) were blended in 200 ml of PBS solution with 300 mM sucrose, and the blended solution was filtered through a 20-μm nylon mesh. After first centrifugation (3850 rpm, 20 min), chloroplast pellet was restored by discarding supernatant and then adding 5 mM $MgCl_2$ contained in PBS solution for the sonication. During the sonication, chloroplast membranes were punctured, and thylakoids were extracted from the chloroplasts. Two centrifugations (3800 rpm, 20 min and 20,000 rpm, 20 min) were done for dilution of $MgCl_2$ in a solution. Aggregated thylakoid pellet was homogenized by glass tissue grinders in a PBS solution with 1.8 M sucrose. For density gradient centrifugation, 1.3 M sucrose contained in PBS solution was carefully stacked on the homogenized thylakoid solution and this layered solution was centrifuged at 38,000 rpm for 1 hour. Because of the density differences between thylakoids and solutions, pure thylakoid layer was formed between two solutions.

Thylakoid deposition on the electrodes

To deposit a uniform amount of thylakoids on the electrodes, chlorophyll concentration in thylakoid solution was calibrated by measuring the light absorbance with an ultraviolet-visible spectrometer (product no. V-650, JASCO Corporation, USA) (*69*). Here, 30 μl of thylakoid droplets with chlorophyll concentration of 2 mg ml^{-1} were dropped on the 1-cm^2 electrodes and dried at room temperature for more than 3 hours.

Electrochemical measurements

In this work, a three-electrode system was used for the electrochemical measurements. Pt mesh and Ag/AgCl (saturated KCl) were used as counter and reference electrode, respectively. To reduce optical and electrical noises during experiments, electrodes were located in a custom-built metallic dark box, which was used as a Faraday cage. All the electrochemical experiments were performed using a potentiostat (CompactStat, Ivium Technologies, The Netherlands) that was controlled by IviumSoft program. For photocurrent generation, light was illuminated by a 100-W halogen lamp (LG-PS2, Olympus, Japan), and its intensity was measured by an optical power meter (product no. 8230E-82311B, ADC Corp., Japan). To measure the potential of electrodes, with PBS solution containing 300 mM potassium nitrate and 30 min of waiting for the saturation, electrode potentials versus Ag/AgCl reference electrode were measured. All the photocurrent measurements except for those mentioned otherwise were carried out with 400 mV versus Ag/AgCl of bias potential and light intensity of 10 mW cm^{-2}.

In situ x-ray absorption spectroscopy measurement

The changes in the local structures of the RuO_2-thylakoid and bare RuO_2 films under light illumination were investigated with EXAFS analyses at Ru K-edge. The present x-ray absorption spectroscopy (XAS) spectra were measured using the EXAFS facility equipped with a beam line 10C at the Pohang Light Source (Pohang, Korea), in which the voltage and current of a synchrotron electron beam were 3.0 GeV and 350 mA, respectively. The same electrochemical condition as mentioned above was carried out simultaneously with the XAS measurement and detected with a fluorescence detector. In the EXAFS fitting analysis, the CNs were fixed to the values on the basis of the crystallographic information of α-$NaRuO_2$ structure, which gave the reasonable values of amplitude reduction factor (S_0^2). In the course of EXAFS fitting analysis, all the parameters of R, Debye-Waller factors (σ^2), and energy shift (ΔE) were set as variables.

Photosynthetic fuel cell

Fuel cell was fabricated by 3 of acrylic compartments based on previous study (*70*). 1.5 ml of PBS solution with 300 mM of KNO_3 was used for minimizing ionic resistance and all experiments were performed in a sealed faraday cage that is filled with oxygen.

SUPPLEMENTARY MATERIALS

Supplementary material for this article is available at http://advances.sciencemag.org/cgi/content/full/7/20/eabf2543/DC1

REFERENCES AND NOTES

1. R. Emerson, R. Chalmers, C. Cederstrand, Some factors influencing the long-wave limit of photosynthesis. *Proc. Natl. Acad. Sci. U.S.A.* **43**, 133–143 (1957).
2. D. Gust, T. A. Moore, Mimicking photosynthesis. *Science* **244**, 35–41 (1989).
3. W. Ryu, S.-J. Bai, J. S. Park, Z. Huang, J. Moseley, T. Fabian, R. J. Fasching, A. R. Grossman, F. B. Prinz, Direct extraction of photosynthetic electrons from single algal cells by nanoprobing system. *Nano Lett.* **10**, 1137–1143 (2010).
4. L. H. Kim, Y. J. Kim, H. Hong, D. Yang, M. Han, G. Yoo, H. W. Song, Y. Chae, J. C. Pyun, A. R. Grossman, W. Ryu, Patterned nanowire electrode array for direct extraction of photosynthetic electrons from multiple living algal cells. *Adv. Funct. Mater.* **26**, 7679–7689 (2016).
5. H. Hong, Y. J. Kim, M. Han, G. Yoo, H. W. Song, Y. Chae, J.-C. Pyun, A. R. Grossman, W. Ryu, Prolonged and highly efficient intracellular extraction of photosynthetic electrons from single algal cells by optimized nanoelectrode insertion. *Nano Res.* **11**, 397–409 (2018).
6. Y. J. Kim, J. Yun, S. I. Kim, H. Hong, J.-H. Park, J.-C. Pyun, W. Ryu, Scalable long-term extraction of photosynthetic electrons by simple sandwiching of nanoelectrode array with densely-packed algal cell film. *Biosens. Bioelectron.* **117**, 15–22 (2018).
7. N. Sekar, Y. Umasankar, R. P. Ramasamy, Photocurrent generation by immobilized cyanobacteria via direct electron transport in photo-bioelectrochemical cells. *Phys. Chem. Chem. Phys.* **16**, 7862–7871 (2014).
8. N. Sekar, R. Jain, Y. Yan, R. P. Ramasamy, Enhanced photo-bioelectrochemical energy conversion by genetically engineered cyanobacteria. *Biotechnol. Bioeng.* **113**, 675–679 (2016).
9. M. Sawa, A. Fantuzzi, P. Bombelli, C. J. Howe, K. Hellgardt, P. J. Nixon, Electricity generation from digitally printed cyanobacteria. *Nat. Commun.* **8**, 1327 (2017).
10. G. Saper, D. Kallmann, F. Conzuelo, F. Zhao, T. N. Tóth, V. Liveanu, S. Meir, J. Szymanski, A. Aharoni, W. Schuhmann, A. Rothschild, G. Schuster, N. Adir, Live cyanobacteria produce photocurrent and hydrogen using both the respiratory and photosynthetic systems. *Nat. Commun.* **9**, 2168 (2018).
11. N. Terasaki, N. Yamamoto, T. Hiraga, Y. Yamanoi, T. Yonezawa, H. Nishihara, T. Ohmori, M. Sakai, M. Fujii, A. Tohri, M. Iwai, Y. Inoue, S. Yoneyama, M. Minakata, I. Enami, Plugging a molecular wire into photosystem I: Reconstitution of the photoelectric conversion system on a gold electrode. *Angew. Chem. Int. Ed.* **48**, 1585–1587 (2009).
12. G. LeBlanc, G. Chen, E. A. Gizzie, G. K. Jennings, D. E. Cliffel, Enhanced photocurrents of photosystem I films on p-doped silicon. *Adv. Mater.* **24**, 5959–5962 (2012).
13. G. LeBlanc, E. Gizzie, S. Yang, D. E. Cliffel, G. K. Jennings, Photosystem I protein films at electrode surfaces for solar energy conversion. *Langmuir* **30**, 10990–11001 (2014).
14. E. A. Gizzie, J. S. Niezgoda, M. T. Robinson, A. G. Harris, G. K. Jennings, S. J. Rosenthal, D. E. Cliffel, Photosystem I-polyaniline/TiO_2 solid-state solar cells: Simple devices for biohybrid solar energy conversion. *Energ. Environ. Sci.* **8**, 3572–3576 (2015).
15. A. Efrati, R. Tel-Vered, D. Michaeli, R. Nechushtai, I. Willner, Cytochrome c-coupled photosystem I and photosystem II (PSI/PSII) photo-bioelectrochemical cells. *Energ. Environ. Sci.* **6**, 2950–2956 (2013).
16. F. Zhao, K. Sliozberg, M. Rögner, N. Plumeré, W. Schuhmann, The role of hydrophobicity of Os-complex-modified polymers for photosystem 1 based photocathodes. *J. Electrochem. Soc.* **161**, H3035–H3041 (2014).
17. E. Darby, G. LeBlanc, E. A. Gizzie, K. M. Winter, G. K. Jennings, D. E. Cliffel, Photoactive films of photosystem I on transparent reduced graphene oxide electrodes. *Langmuir* **30**, 8990–8994 (2014).
18. J. Maly, J. Masojidek, A. Masci, M. Ilie, E. Cianci, V. Foglietti, W. Vastarella, R. Pilloton, Direct mediatorless electron transport between the monolayer of photosystem II and poly (mercapto-p-benzoquinone) modified gold electrode—New design of biosensor for herbicide detection. *Biosens. Bioelectron.* **21**, 923–932 (2005).
19. O. Yehezkeli, R. Tel-Vered, J. Wasserman, A. Trifonov, D. Michaeli, R. Nechushtai, I. Willner, Integrated photosystem II-based photo-bioelectrochemical cells. *Nat. Commun.* **3**, 742 (2012).

20. J. Li, X. Feng, J. Fei, P. Cai, J. Huang, J. Li, Integrating photosystem II into a porous TiO_2 nanotube network toward highly efficient photo-bioelectrochemical cells. *J. Mater. Chem. A* **4**, 12197–12204 (2016).
21. J. O. Calkins, Y. Umasankar, H. O'Neill, R. P. Ramasamy, High photo-electrochemical activity of thylakoid–carbon nanotube composites for photosynthetic energy conversion. *Energy. Environ. Sci.* **6**, 1891–1900 (2013).
22. M. Rasmussen, A. Shrier, S. D. Minteer, High performance thylakoid bio-solar cell using laccase enzymatic biocathodes. *Phys. Chem. Chem. Phys.* **15**, 9062–9065 (2013).
23. K. Hasan, Y. Dilgin, S. C. Emek, M. Tavahodi, H. E. Åkerlund, P. Å. Albertsson, L. Gorton, Photoelectrochemical communication between thylakoid membranes and gold electrodes through different quinone derivatives. *ChemElectroChem* **1**, 131–139 (2014).
24. G. Pankratova, D. Pankratov, K. Hasan, H. E. Åkerlund, P. Å. Albertsson, D. Leech, S. Shleev, L. Gorton, Supercapacitive photo-bioanodes and biosolar cells: A novel approach for solar energy harnessing. *Adv. Energy Mater.* **7**, 1602285 (2017).
25. A.-I. Bunea, A. Heiskanen, G. Pankratova, G. Tesei, M. Lund, H.-E. Åkerlund, D. Leech, N. B. Larsen, S. Sylvest Keller, L. Gorton, J. Emnéus, Micropatterned carbon-on-quartz electrode chips for photocurrent generation from thylakoid membranes. *ACS Appl. Energy Mater.* **1**, 3313–3322 (2018).
26. N. D. Kirchhofer, M. A. Rasmussen, F. W. Dahlquist, S. D. Minteer, G. C. Bazan, The photobioelectrochemical activity of thylakoid bioanodes is increased via photocurrent generation and improved contacts by membrane-intercalating conjugated oligoelectrolytes. *Energ. Environ. Sci.* **8**, 2698–2706 (2015).
27. M. Rasmussen, S. D. Minteer, Thylakoid direct photobioelectrocatalysis: Utilizing stroma thylakoids to improve bio-solar cell performance. *Phys. Chem. Chem. Phys.* **16**, 17327–17331 (2014).
28. H. Hamidi, K. Hasan, S. C. Emek, Y. Dilgin, H. E. Åkerlund, P. Å. Albertsson, D. Leech, L. Gorton, Photocurrent generation from thylakoid membranes on osmium-redox-polymer-modified electrodes. *ChemSusChem* **8**, 990–993 (2015).
29. X. Zhou, L. Zhou, P. Zhang, F. Lv, L. Liu, R. Qi, Y. Wang, M. Y. Shen, H. H. Yu, G. Bazan, S. Wang, Conducting polymers–thylakoid hybrid materials for water oxidation and photoelectric conversion. *Adv. Electron. Mater.* **5**, 1800789 (2019).
30. X. Zhou, P. Gai, P. Zhang, H. Sun, F. Lv, L. Liu, S. Wang, Conjugated polymer enhanced photoelectric response of self-circulating photosynthetic bioelectrochemical cell. *ACS Appl. Mater. Interfaces* **11**, 38993–39000 (2019).
31. H. Kanso, G. Pankratova, P. Bollella, D. Leech, D. Hernandez, L. Gorton, Sunlight photocurrent generation from thylakoid membranes on gold nanoparticle modified screen-printed electrodes. *J. Electroanal. Chem.* **816**, 259–264 (2018).
32. D. Pankratov, G. Pankratova, T. P. Dyachkova, P. Falkman, H.-E. Åkerlund, M. D. Toscano, Q. Chi, L. Gorton, Supercapacitive biosolar cell driven by direct electron transfer between photosynthetic membranes and CNT networks with enhanced performance. *ACS Energy Lett.* **2**, 2635–2639 (2017).
33. P. Cai, G. Li, Y. Yang, X. Su, Z. Zhang, Co-assembly of thylakoid and graphene oxide as a photoelectrochemical composite film for enhanced mediated electron transfer. *Colloids Surf. A Physicochem. Eng. Asp.* **555**, 37–42 (2018).
34. D. Pankratov, J. Zhao, M. A. Nur, F. Shen, D. Leech, Q. Chi, G. Pankratova, L. Gorton, The influence of surface composition of carbon nanotubes on the photobioelectrochemical activity of thylakoid bioanodes mediated by osmium-complex modified redox polymer. *Electrochim. Acta* **310**, 20–25 (2019).
35. J. M. Anderson, Lateral heterogeneity of plant thylakoid protein complexes: Early reminiscences. *Philos. Trans. R. Soc. Lond. B Biol. Sci.* **367**, 3384–3388 (2012).
36. F. A. Armstrong, H. A. O. Hill, N. J. Walton, Direct electrochemistry of redox proteins. *Acc. Chem. Res.* **21**, 407–413 (1988).
37. J. E. Frew, H. A. O. Hill, Direct and indirect electron transfer between electrodes and redox proteins. *Eur. J. Biochem.* **172**, 261–269 (1988).
38. S. R. Crittenden, C. J. Sund, J. J. Sumner, Mediating electron transfer from bacteria to a gold electrode via a self-assembled monolayer. *Langmuir* **22**, 9473–9476 (2006).
39. K. B. Lam, E. F. Irwin, K. E. Healy, L. Lin, Bioelectrocatalytic self-assembled thylakoids for micro-power and sensing applications. *Sens. Actuat. B Chem.* **117**, 480–487 (2006).
40. J. Pawlowski, J. Juhaniewicz, D. Tymecka, S. Sek, Electron transfer across α-helical peptide monolayers: Importance of interchain coupling. *Langmuir* **28**, 17287–17294 (2012).
41. H. Over, Surface chemistry of ruthenium dioxide in heterogeneous catalysis and electrocatalysis: From fundamental to applied research. *Chem. Rev.* **112**, 3356–3426 (2012).
42. C. Zhan, D.-e. Jiang, Understanding the pseudocapacitance of RuO_2 from joint density functional theory. *J. Phys. Condens. Matter* **28**, 464004 (2016).
43. S. Chalupczok, P. Kurzweil, H. Hartmann, C. Schell, The redox chemistry of ruthenium dioxide: A cyclic voltammetry study—Review and revision. *Int. J. Electrochem* **2018**, 1273768 (2018).
44. J. Barber, Influence of surface charges on thylakoid structure and function. *Annu. Rev. Plant Biol.* **33**, 261–295 (1982).
45. R. Fristedt, P. Granath, A. V. Vener, A protein phosphorylation threshold for functional stacking of plant photosynthetic membranes. *PLOS ONE* **5**, e10963 (2010).
46. K. Fukuda, T. Saida, J. Sato, M. Yonezawa, Y. Takasu, W. Sugimoto, Synthesis of nanosheet crystallites of ruthenate with an α-$NaFeO_2$-related structure and its electrochemical supercapacitor property. *Inorg. Chem.* **49**, 4391–4393 (2010).
47. C. Santoro, F. Soavi, A. Serov, C. Arbizzani, P. Atanassov, Self-powered supercapacitive microbial fuel cell: The ultimate way of boosting and harvesting power. *Biosens. Bioelectron.* **78**, 229–235 (2016).
48. M. Kato, T. Cardona, A. W. Rutherford, E. Reisner, Photoelectrochemical water oxidation with photosystem II integrated in a mesoporous indium–tin oxide electrode. *J. Am. Chem. Soc.* **134**, 8332–8335 (2012).
49. K. Brinkert, F. Le Formal, X. Li, J. Durrant, A. W. Rutherford, A. Fantuzzi, Photocurrents from photosystem II in a metal oxide hybrid system: Electron transfer pathways. *Biochim. Biophys. Acta* **1857**, 1497–1505 (2016).
50. M. Rasmussen, S. D. Minteer, Investigating the mechanism of thylakoid direct electron transfer for photocurrent generation. *Electrochim. Acta* **126**, 68–73 (2014).
51. X. Bao, Y. Zhang, J. Wang, D. Zhu, C. Yang, Y. Li, C. Yang, J. Xu, R. Yang, High extinction coefficient thieno [3, 4-b] thiophene-based copolymer for efficient fullerene-free solar cells with large current density. *Chem. Mater.* **29**, 6766–6771 (2017).
52. K. H. Sjöholm, M. Rasmussen, S. D. Minteer, Bio-solar cells incorporating catalase for stabilization of thylakoid bioelectrodes during direct photoelectrocatalysis. *ECS Elctrchem. Lett.* **1**, G7–G9 (2012).
53. J. Lee, J. Im, S. Kim, Mediatorless solar energy conversion by covalently bonded thylakoid monolayer on the glassy carbon electrode. *Bioelectrochemistry* **108**, 21–27 (2016).
54. O. E. Castañeda Ocampo, P. Gordiichuk, S. Catarci, D. A. Gautier, A. Herrmann, R. C. Chiechi, Mechanism of orientation-dependent asymmetric charge transport in tunneling junctions comprising photosystem I. *J. Am. Chem. Soc.* **137**, 8419–8427 (2015).
55. L. A. Dick, A. J. Haes, R. P. Van Duyne, Distance and orientation dependence of heterogeneous electron transfer: A surface-enhanced resonance raman scattering study of cytochrome *c* bound to carboxylic acid terminated alkanethiols adsorbed on silver electrodes. *J. Phys. Chem. B* **104**, 11752–11762 (2000).
56. M. Kato, T. Cardona, A. W. Rutherford, E. Reisner, Covalent immobilization of oriented photosystem II on a nanostructured electrode for solar water oxidation. *J. Am. Chem. Soc.* **135**, 10610–10613 (2013).
57. Y. Umena, K. Kawakami, J.-R. Shen, N. Kamiya, Crystal structure of oxygen-evolving photosystem II at a resolution of 1.9 Å. *Nature* **473**, 55–60 (2011).
58. L. Frolov, O. Wilner, C. Carmeli, I. Carmeli, Fabrication of oriented multilayers of photosystem I proteins on solid surfaces by auto-metallization. *Adv. Mater.* **20**, 263–266 (2008).
59. H. Käss, P. Fromme, H. T. Witt, W. Lubitz, Orientation and electronic structure of the primary donor radical cation in photosystem I: A single crystals EPR and ENDOR study. *J. Phys. Chem. B* **105**, 1225–1239 (2001).
60. M. Ciobanu, H. A. Kincaid, V. Lo, A. D. Dukes, G. K. Jennings, D. E. Cliffel, Electrochemistry and photoelectrochemistry of photosystem I adsorbed on hydroxyl-terminated monolayers. *J. Electroanal. Chem.* **599**, 72–78 (2007).
61. J. Tsukada, H. Ozawa, S. Uno, K. Nakazato, N. Terasaki, N. Yamamoto, T. Hiraga, M. Iwai, M. Konno, K. Ito, Y. Inoue, Photosystem I bio-photosensor integrated with complementary metal–oxide–semiconductor source–drain follower on a chip. *Jpn. J. Appl. Phys.* **49**, 01AG04 (2010).
62. M. A. Harmer, H. Allen, O. Hill, The direct electrochemistry of redox proteins at metal oxide electrodes. *J. Electroanal. Chem.* **189**, 229–246 (1985).
63. E. L. Gross, Plastocyanin: Structure, location, diffusion and electron transfer mechanisms, in *Oxygenic Photosynthesis: The Light Reactions* (Springer, 1996), pp. 413–429.
64. J. M. Guss, H. D. Bartunik, H. C. Freeman, Accuracy and precision in protein structure analysis: Restrained least-squares refinement of the structure of poplar plastocyanin at 1.33 Å resolution. *Acta Crystallogr. B* **48**, 790–811 (1992).
65. F. A. Armstrong, H. Allen, O. Hill, N. J. Walton, Reactions of electron-transfer proteins at electrodes. *Q. Rev. Biophys.* **18**, 261–322 (1985).
66. E. D. Duée, E. Fanchon, J. Vicat, L. C. Sieker, J. Meyer, J.-M. Moulis, Refined crystal structure of the 2 [4Fe-4S] ferredoxin from Clostridium acidurici at 1.84 Å resolution. *J. Mol. Biol.* **243**, 683–695 (1994).
67. M. T. Bes, E. Parisini, L. A. Inda, L. M. Saraiva, M. L. Peleato, G. M. Sheldrick, Crystal structure determination at 1.4 Å resolution of ferredoxin from the green alga Chlorella fusca. *Structure* **7**, 1201–12S2 (1999).
68. I. Daizadeh, D. M. Medvedev, A. A. Stuchebrukhov, Electron transfer in ferredoxin: Are tunneling pathways evolutionarily conserved? *Mol. Biol. Evol.* **19**, 406–415 (2002).
69. D. I. Arnon, Copper enzymes in isolated chloroplasts. Polyphenoloxidase in Beta vulgaris. *Plant Physiol.* **24**, 1–15 (1949).
70. D. Ryu, Y. J. Kim, S. I. Kim, H. Hong, H. S. Ahn, K. Kim, W. Ryu, Thylakoid-deposited micro-pillar electrodes for enhanced direct extraction of photosynthetic electrons. *Nanomaterials* **8**, 189 (2018).
71. M. Fayette, A. Nelson, R. D. Robinson, Electrophoretic deposition improves catalytic performance of Co_3O_4 nanoparticles for oxygen reduction/oxygen evolution reactions. *J. Mater. Chem. A* **3**, 4274–4283 (2015).

72. D. R. Sandstrom, EXAFS studies of electrolyte solutions, in *EXAFS and Near Edge Structure III* (Springer, 1984), pp. 409–413.
73. P. Chernev, S. Fischer, J. Hoffmann, N. Oliver, R. Assunção, B. Yu, R. L. Burnap, I. Zaharieva, D. J. Nürnberg, M. Haumann, H. Dau, Light-driven formation of manganese oxide by today's photosystem II supports evolutionarily ancient manganese-oxidizing photosynthesis. *Nat. Commun.* **11**, 6110 (2020).

Acknowledgments: The experiments at PAL were supported, in part, by MOST and POSTECH. **Funding:** This research was supported by the National Research Foundation of Korea (NRF) grant funded by the Korea Government (MSIP) (nos. NRF-2020R1A2C3013158 and NRF-2020R1A2C3008671). **Author contributions:** H.H., J.M.L., S.-J.H., and W.R. designed and developed the concept and the experiments, as well as wrote the manuscript. In the experiments, H.H. and J.Y. performed electrochemical measurements, and J.M.L. performed RuO_2 NS exfoliation and EXAFS measurements. Y.J.K., S.I.K., and H.S. performed thylakoid isolation, investigated NS deposition, and constructed photosynthetic electrochemical cells. H.H., J.M.L., H.S.A., S.-J.H., and W.R. analyzed and discussed electrochemical data. **Competing interests:** The authors declare that they have no competing interests. **Data and materials availability:** All data needed to evaluate the conclusions in the paper are present in the paper and/or the Supplementary Materials. Additional data related to this paper may be requested from the authors.

Submitted 15 October 2020
Accepted 29 March 2021
Published 12 May 2021
10.1126/sciadv.abf2543

Citation: H. Hong, J. M. Lee, J. Yun, Y. J. Kim, S. I. Kim, H. Shin, H. S. Ahn, S.-J. Hwang, W. Ryu, Enhanced interfacial electron transfer between thylakoids and RuO_2 nanosheets for photosynthetic energy harvesting. *Sci. Adv.* **7**, eabf2543 (2021).